the plant journal

SEB Society for Experimental Biology

The Plant Journal (2014) **80,** 553–567 doi: 10.1111/tpj.12639

TECHNICAL ADVANCE

Significant reduction of BiFC non-specific assembly facilitates *in planta* assessment of heterotrimeric G-protein interactors

Timothy E. Gookin and Sarah M. Assmann*

Department of Biology, The Pennsylvania State University, University Park, PA 16802, USA

Received 29 April 2014; revised 29 July 2014; accepted 4 August 2014; published online 4 September 2014.
*For correspondence (e-mail sma3@psu.edu).

SUMMARY

Protein networks and signaling cascades are key mechanisms for intra- and intercellular signal transduction. Identifying the interacting partners of a protein can provide vital clues regarding its physiological role. The bimolecular fluorescence complementation (BiFC) assay has become a routine tool for *in vivo* analysis of protein–protein interactions and their subcellular location. Although the BiFC system has improved since its inception, the available options for *in planta* analysis are still subject to very low signal-to-noise ratios, and a systematic comparison of BiFC confounding background signals has been lacking. Background signals can obscure weak interactions, provide false positives, and decrease confidence in true positives. To overcome these problems, we performed an extensive *in planta* analysis of published BiFC fragments used in metazoa and plants, and then developed an optimized single vector BiFC system which utilizes monomeric Venus (mVenus) split at residue 210, and contains an integrated mTurquoise2 marker to precisely identify transformed cells in order to distinguish true negatives. Here we provide our streamlined double ORF expression (pDOE) BiFC system, and show that our advance in BiFC methodology functions even with an internally fused mVenus210 fragment. We illustrate the efficacy of the system by providing direct visualization of Arabidopsis MLO1 interacting with a calmodulin-like (CML) protein, and by showing that heterotrimeric G-protein subunits Gα (GPA1) and Gβ (AGB1) interact in plant cells. We further demonstrate that GPA1 and AGB1 each physically interact with PLDα1 *in planta*, and that mutation of the so-called PLDα1 'DRY' motif abolishes both of these interactions.

Keywords: bimolecular fluorescence complementation, protein–protein interaction, heterotrimeric G-proteins, phospholipase, calmodulin, protoplast transformation, agroinfiltration, *Arabidopsis thaliana*, *Nicotiana benthamiana*, technical advance.

INTRODUCTION

Microscopy-based bimolecular fluorescence complementation (BiFC) has the tremendous advantage of allowing simultaneous assessment of protein–protein interactions and determination of their subcellular localization. The most commonly used BiFC systems, however, are prone to false positives due to both reassembly of the fluoroprotein fragments even in the absence of interaction of the test proteins and the inherent tendency of the fluoroprotein to dimerize (Lalonde *et al.*, 2008; Kodama and Hu, 2012). *Aequorea* derived GFP derivatives such as Venus are approximately 239 residues long and are characterized by 11 β-sheets which fold into a β-barrel structure with a central chromophore. For BiFC, the yellow fluorescent protein Venus is commonly split between the seventh and eighth β-sheets at residue 155, split between the eighth and ninth β-sheet at residue 173, or split using an overlap strategy to increase signal strength wherein the N-terminal fragment (NVen) is created from residues 1–173 and paired with the C-terminal (CVen) 155–239 fragment (Kodama and Hu, 2012). Split neatly at residue 155, each half adopts opposed U-shaped structures which interlace to reconstitute the three-dimensional (3-D) β-barrel (Isogai *et al.*, 2011). In the overlap pair, the eighth β-sheet is duplicated and the exact placement of the additional sheet in the 3-D structure is unknown.

Spontaneous assembly of NVen and CVen provides a source of false positives and confounds signals originating

from true interactions. Cells experiencing physiological distress, or cells assayed at late timepoints when fusion proteins are in high concentration can accrue high levels of mislocalized fluorescent signal (Kerppola, 2006; Vahisalu *et al.*, 2010). Clear examples are provided by SLAC1, a plasma membrane-localized anion channel, which showed nuclear BiFC signal in an interaction assay (Vahisalu *et al.*, 2010), the false-positive signal produced by the tomato NEVER-RIPE receptor and a mutated form of LeCTR3, and the self-assembly between wild-type LeCTR3:CVen and an unfused NVen fragment (Zhong *et al.*, 2008). Skilled researchers familiar with BiFC and employing multiple types of controls (e.g. multiple plants, a range of infiltration concentrations, and time-course observations) can usually identify problematic assays, but some false positives can easily mimic the signal intensity of a true protein–protein interaction. Fusing a non-target protein to one Venus fragment can reduce the background signal intensity observed in negative controls, but this effect can be protein specific. For example, a very large non-target control protein fused to CVen may simply physically block access to the fragment, while another non-target control protein choice might interfere with CVen β-sheet formation. In either case the control protein would always provide negative BiFC data, but neither control would accurately reflect the inherent self-assembly potential of the system, nor provide an appropriate reference for qualitatively judging the strength of true interactions. Negating a positive interaction by an introduced point mutation is a 'gold standard' control, but this is impractical when performing large interaction screens and daunting when obvious interaction domains are lacking. Therefore, controls wherein the second Venus fragment remains unfused are optimal.

Experiments with the goal of reducing the spontaneous assembly of NVen and CVen in animal systems have focused on introducing additional point mutations to the last few residues of the seventh β-sheet of NVen, and have been performed in *Xenopus* embryos, HEK293T cells, HeLa cells, and COS-1 cells. Results ranging from increased signal-to-noise ratios to the loss of the BiFC signal showed that the effects of the V150L, I152L, and T153M mutations are highly context dependent. For example, the V150L mutation increased the signal-to-noise (S/N) ratio in an NVen158 fragment (Lin *et al.*, 2010) but nearly eliminated the authentic BiFC signal when present in an NVen155 fragment (Kodama and Hu, 2010). The I152L mutation increased the S/N ratio in the monomeric Venus (mVenus) 155/155 and 173/173 fragment pairs, but not in the 173/155 overlapping fragment pair, and this optimization was not transferable to the very similar blue fluoroprotein Cerulean (Kodama and Hu, 2010). The T153M mutation could reduce background signal in *Xenopus* cells, and to a slight degree in COS-1 cells, but it only optimized the S/N ratio in *Xenopus* cells (Saka *et al.*, 2007; Kodama and Hu, 2010). An alternative approach to reduce self-assembly was performed by creating a mutation in the 10th β-sheet (L201V) at a position predicted to interact with V150 and V152; this mutation increased the S/N ratio in mouse C3H10T1/2 cells but also decreased the overall efficiency of BiFC (Nakagawa *et al.*, 2011). Collectively it appears that targeting the tail of the NVen155 fragment is a moderately successful approach, but retaining the sensitivity to detect weak interactions while simultaneously reducing background noise may not be fully realized.

Recently, Ohashi *et al.* (2012) exhaustively assayed BiFC system performance in HeLa cells by independently splitting Venus between each of the 11 β-sheets and assessing 91 unfused fragment pairs for fluorescence. While none of the fragments fluoresced alone, 44 combinations of the two halves, unfused to any interacting proteins, exhibited some spontaneous fluorescence. Subsequent analysis of 1456 interaction pairs comprising the various split Venus fragments fused to actin and either cofilin or a non-interacting cofilin point mutant identified N-terminal fusions of Venus split at residue 210 as the most discriminatory combination of fragments. Similar to a strategy used to split superfolder GFP (Zhou *et al.*, 2011), this split position substantially reduces the size of the CVen fragment to the 29 residues which compose the 11th β-sheet and trailing terminal residues.

Additional issues with currently available BiFC systems involve vector utilization and implementation. Many systems are flexible in matrix style analyses, but require subcloning into an entry vector before creating test constructs. Moreover, systems that require mixing plasmids or *Agrobacterium* cultures for co-transformation inevitably lead to stochastic expression cassette concentrations within individual cells due to unequal transformation events. Furthermore, unrecombined Gateway cloning cassettes do not allow translational read-through to downstream fluoroprotein fragments, therefore the self-assembly potential cannot be assessed in any orientation other than the combination of two N-terminal tag cassettes.

To assist in resolving all of the above issues, we sought to create a 'zero background' BiFC system that facilitates interaction screens in a one-to-many configuration. In our system, two expression cassettes with identical promoters are placed within the same vector and cloning is performed directly in the binary vector via multiple cloning sites (MCS). Once the gene-of-interest is cloned into the first expression cassette, the vector becomes a 'parent vector' into which all of the putative interacting partners may be directly inserted. The parent vector is not simply an intermediate step as the parent vector also constitutes a true negative control for all downstream interactions; it provides a direct measure of the in-context stickiness of the BiFC halves as well as of the general ability of the protein of interest to bring the two halves of mVenus together.

While developing our single vector analytical system, we found that, analogous to the situation described above for assays in mammalian cells, the Venus BiFC fragment halves employed in currently available plant BiFC systems often produce unacceptable levels of background fluorescence that obscure weak interactions and/or tightly spatially constrained signals. Importantly, all of the prior systems that we tested showed extensive non-specific signal when one of the Venus halves was left unfused, and all accrued non-specific signal over time. After extensive investigation of the most recent BiFC fragment pairs and point mutations utilized in metazoan systems, we identified mVenus split at residue 210 to be a highly discriminatory pair, with nearly zero background signal accrual in plant cells even at extended timepoints and when one Venus fragment remained unfused to a plant protein.

Accordingly, we utilized mVenus split at residue 210 to create multiple sets of four double ORF expression vectors that allow all N- and C-terminal fusion proteins to be made, with options to express these cassettes using a 35S promoter or a Ubiquitin10 promoter, which has lower activity in *Nicotiana benthamiana* (Grefen *et al.*, 2010). Our single vector design allows for efficient BiFC experimentation via agroinfiltration, protoplast transformation, and biolistic bombardment. An integrated Golgi-localized mTurquoise2 (mTq2) transformation control allows for the identification of transformed cells, which is highly important for determination of a genuinely negative BiFC result. To provide a means to further characterize positive protein–protein interactions in BiFC assays via FRET, or to perform subcellular co-localization in plant cells, we also created a compatible dual expression vector set that enables all N- and C-terminal fusion combinations with mTq2 and mVenus, which are currently the brightest and longest lived cyan and yellow fluoroproteins available (Goedhart *et al.*, 2010).

Using our new BiFC system we show that MLO1, a protein known to interact with typical calmodulins (CaMs) (Kim *et al.*, 2002), can interact with CaM1 as well as with the divergent calmodulin-like 40 protein (CML40). We show the formation of βγ dimers between the Arabidopsis heterotrimeric Gβ (AGB1) and all three Gγ subunits (AGG1, AGG2, and AGG3) *in planta.* Importantly, we provide direct in-plant visualization of the heterotrimeric Gα subunit (GPA1) interacting with AGB1; an interaction which we show to be spatially constrained and highly dependent on the presence of a Gγ subunit. We demonstrate that GPA1 interacts *in planta* with PLDα1 but not with residue substitution mutants of the identified 'DRY' motif previously shown to be critical for GPA1–PLDα1 binding *in vitro* (Zhao and Wang, 2004). We also extend the connection between plant G-protein and phospholipase D signaling by showing that PLDα1 also interacts with AGB1, but only when AGB1 is complexed in a Gβγ dimer.

RESULTS AND DISCUSSION

Assessment of mVenus 173/155 based BiFC systems

We performed initial BiFC assessments using a Gateway adapted pDEST–VYNE/VYCE BiFC system (Gehl *et al.*, 2009) which employs the widely used 173/155 overlap fragment pair of Venus. Our agroinfiltration experiments successfully confirmed the published homodimerization of Cnx6 (Gehl *et al.*, 2009). We assessed the self-assembly potential of the system using $VYNE^{GW}$::Cnx6, $VYNE^{GW}$::GPA1, $GPA1^{GW}$::VYNE, and MLO1::^{GW}VYNE with unrecombined pDEST–$VYCE(R)^{GW}$. (Note that assays cannot be performed using unrecombined Gateway destination vectors with downstream tags since the Gateway cassette does not allow translational read-through.) We found the self-assembly potential of the Gateway-based 173/155 system was high regardless of the N-terminal tag placement or gene tested (Figure 1).

Reasoning that one issue is the inevitable unequal concentrations of fusion cassettes from unequal co-transformation events, we sought to create a streamlined system that could introduce the expression cassettes into each transformed cell in a 1:1 ratio. We created a single-vector double ORF expression vector (pDOE) BiFC system (see Methods S1 and Figure 2), which we hypothesized would decrease background noise through decreased vector transformation concentrations while simultaneously increasing signal uniformity across individual leaf infiltrations and between independent experiments. The first iteration of our BiFC system employed the same commonly used 173/155 overlap pair of Venus fragments used to develop other BiFC vector systems (Lee *et al.*, 2008; Waadt *et al.*, 2008; Gehl *et al.*, 2009; Berendzen *et al.*, 2012). To test this system, we chose to use the seven transmembrane domain-containing MLO1 protein (At4g02600) and the membrane-associated Gα subunit, GPA1 (At2g26300). These proteins were each inserted into MCS1 to create two parent vectors. Our assessments were limited to C-terminal fusions because the N-terminus of MLO1 is expected to be extracellular, analogous to the topology of barley MLO (Devoto *et al.*, 1999), and GPA1 mislocalized when tagged at the N-terminus (Figure 1c). To provide a positive control, we employed the interaction between MLO1 and CaM1 (At5g37780), a prototypical calmodulin (Figure 3a). Arabidopsis MLO1 binds barley CaM3 in yeast two-hybrid assays, and contains a CaM binding domain (CaMBD) conserved with barley MLO, a protein with functionally significant CaM binding (Kim *et al.*, 2002).

Our initial assessment of the system using the 173/155 overlap pair showed significant non-specific signal for the double empty vector (Figure S1) as well as for the parent vectors that only contained either MLO1 or GPA1 (Figure 3b,c). The non-specific assembly was not appreciably decreased by our single vector design or by our use of the

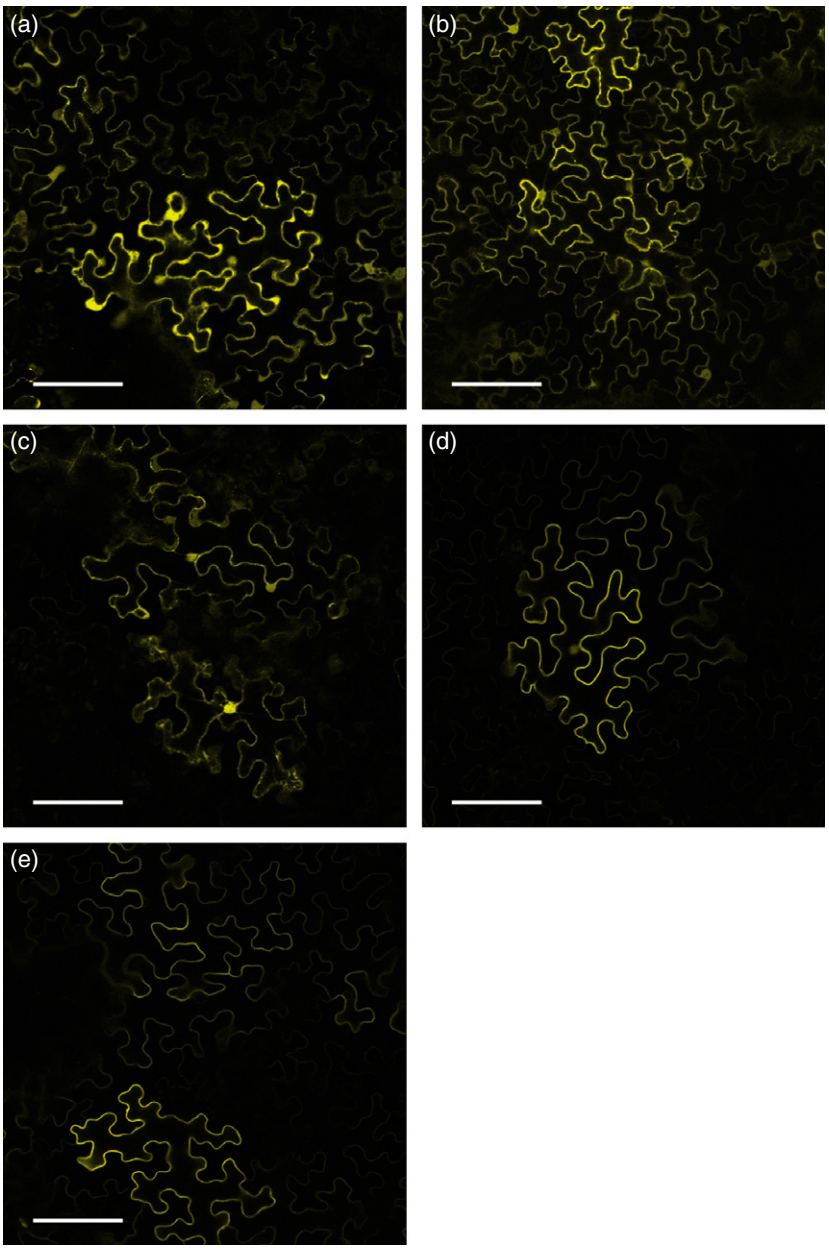

Figure 1. The Gateway adapted 173/155 split Venus BiFC system readily self-assembles when one fragment is left unfused.
(a) VYNE^{GW}::Cnx6 dimerization with VYCE^{GW}::Cnx6 (positive control).
(b) VYNE^{GW}::Cnx6 expressed with unfused VYCE(R)^{GW} (negative control) produces non-specific fluorescence.
(c) VYNE^{GW}::GPA1 expressed with an unfused VYCE(R)^{GW} (negative control) produces fluorescence, some of which mislocalizes to the nucleus.
(d) GPA1::^{GW}VYNE expressed with unfused VYCE(R)^{GW} (negative control) produces fluorescence.
(e) MLO1::^{GW}VYNE expressed with VYCE(R)^{GW} (negative control) produces fluorescence. *Nicotiana benthamiana* leaves were agroinfiltrated at a final optical density of 0.025 for each vector and imaged 46 h later. Scale bars: 100 μm.

Venus A206K mutation, which prevents Venus dimerization (Zacharias *et al.*, 2002; von Stetten *et al.*, 2012); therefore we reasoned that the intrinsic stickiness of the 173/155 pair, rather than dimerization, was the major contributing factor to the non-specific signal.

Assessment of mVenus 155/155 based BiFC systems

The 155/155 Venus fragment pair has been described as being less prone to spontaneous self-assembly than the 173/155 pair, and recently described point mutations in the seventh β-sheet have led to success in optimizing the S/N ratio in metazoan expression systems (Saka *et al.*, 2007; Kodama and Hu, 2010; Lin *et al.*, 2010). By contrast, in onion (*Allium cepa*) cells, the difference between positives and negative for the 155/155 pair were negligible, and the I152L mutation only increased the S/N ratio twofold (Kodama and Hu, 2012). An attempt to reduce non-specific assembly in Arabidopsis protoplasts was performed (Li *et al.*, 2010) and consisted of simultaneously deleting T153 and A154 of N-YFP. Although a S/N ratio was not reported, the deletion appeared to reduce both non-specific assembly and sensitivity since the authors noted that the deletion caused a significant reduction in true BiFC signal despite massive transient overexpression (Li *et al.*, 2010). We modified our pDOE vector to test the native 155/155 split, as well as the V150L, I152L, and T153M point mutations, again using the Arabidopsis MLO1 and CaM1 interaction as the positive control.

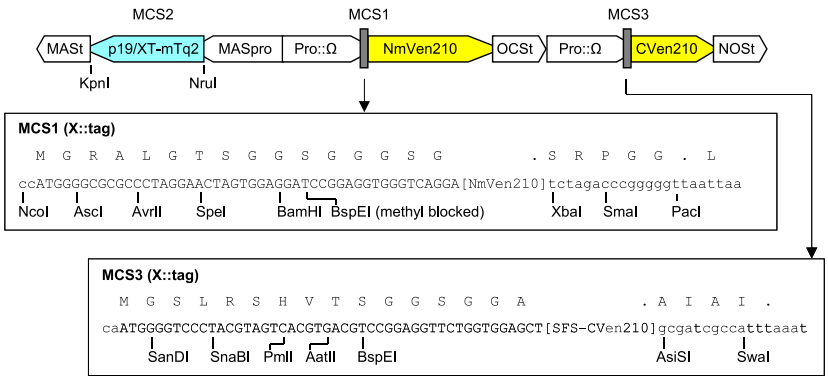

Figure 2. General organizational pattern for the final pDOE vector exemplified using pDOE-01 X::NmVen210–X::CVen210.
Two expression cassettes (MCS1 and MCS3) with identical promoters (either 35S or UBQ10) linked to an Omega translation enhancer (Ω) drive fusion protein expression. BiFC vectors with all four N- and C-terminal fusion combinations are available. Full-length fluoroprotein fusion vectors for dual localization have mTq2 in cassette 1; mVenus in cassette 3. The MAS promoter-driven MCS2 expresses accessory proteins p19 or the XT–Golgi–mTurquoise2 marker. Boxes show the general scheme for linker sequences and restriction site arrangement. SFS–CVen210 in the box for MCS3 shows the position of the StrepII–FLAG–StrepII epitope linker. See Methods S1 and S2 for additional details and schematics.

Figure 3. Integration of the mVenus 173/155 overlap fragment pair into a pDOE vector did not decrease Venus self-assembly in negative controls.
(a) MLO1:NVen173–CaM1:CVen155 construct (positive control).
(b) MLO1:NVen173–X:CVen155 construct (negative control).
(c) GPA1:NVen173–X:CVen155 (negative control). *Nicotiana benthamiana* leaves were agro-infiltrated at an optical density of 0.025 and imaged 48 h later. Scale bar: 100 μm.

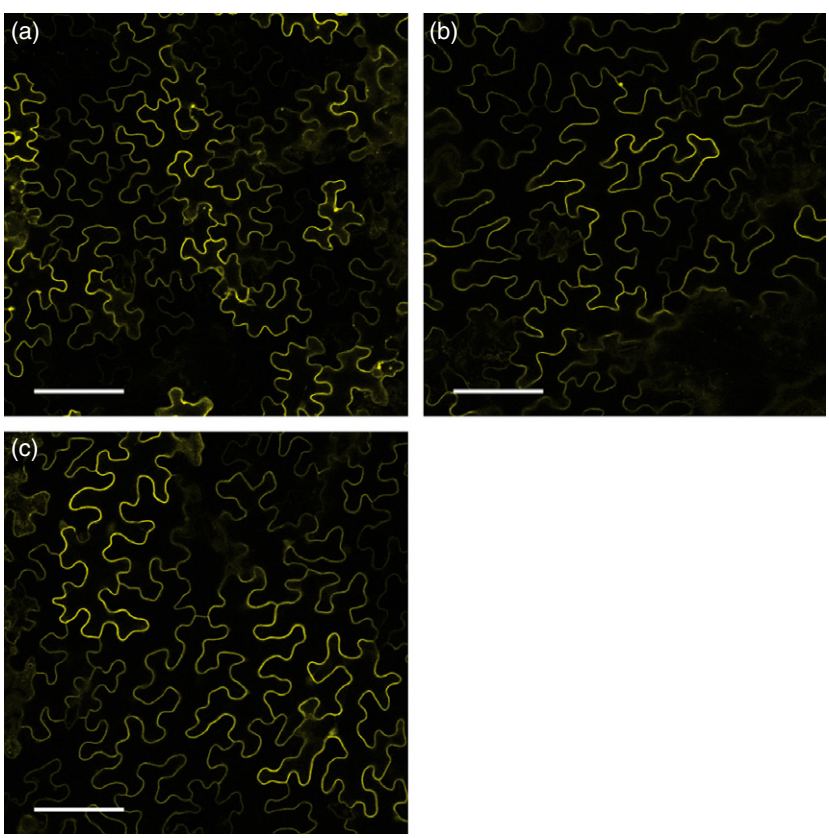

Preliminary screens using our empty base vector with mVenus split at 155/155 did not show any meaningful reduction of baseline signal at later time points, therefore we investigated these constructs closer to the onset of signal appearance. Relatively early time point analysis of the effect of the point mutations in the seventh β-sheet in the 155/155 fragment pair showed that non-specific negative control signals are still present, albeit reduced compared to true protein–protein interaction signal (Figure S2). The reduced positive signal of the 155/155 fragment pair (Figure S2a,b) relative to the 173/155 pair (Figure 3a,b), and the evident false positive signal from V150L, I152L, and T153M mutations in the MLO1:NVen155 fusions expressed with an unfused CmVen155 (Figure S2b–d) meant that none of these 155/155 fragment pairs qualified as the basis for an unambiguous BiFC-based protein–protein interaction system.

Construction of a mVenus 210/210 based BiFC system

Our third iteration of BiFC was performed using mVenus split in the soluble loop between the 10th and 11th β-sheets at residue 210. This split was highly effective in optimizing BiFC in mammalian cells (Ohashi *et al.*, 2012), and, relevant to our experimental focus on G-protein signaling, it has demonstrated success in the interaction of calmodulin and the M13 peptide, and in assays with the small G-protein Ras (Ohashi *et al.*, 2012). We created this newest version of the BiFC base vector by placing the NmVen210 fragment, which contains the A206K monomerizing mutation, downstream of MCS1, and by placing the CVen210 fragment in MCS3 with a preceding StrepII–FLAG–StrepII epitope linker (SFS). Notably, the C-terminal Venus fragment comprises only 29 amino acids of which only the 10 central residues (217–227) create the ordered 11th β-sheet. The unstructured, flexible SFS linker is 40 residues long, includes spacers between each epitope, provides for adequate spatial separation of CVen210 from the target ORF, and presumably assists in overcoming fusion-tag accessibility issues and steric constraints imposed by the assembly of two interacting proteins (Evers *et al.*, 2006; Mal *et al.*, 2007). The bipartite StrepII tag was chosen because it has been used successfully to pull down multi-protein complexes in human cells (Groth *et al.*, 2007) and Arabidopsis leaves (Olinares *et al.*, 2011). Combined with the previously demonstrated ability of the StrepII tag to facilitate isolation of recombinant protein from plants (Witte *et al.*, 2004), the SFS-CVen210 fusion tag should be a multi-functional asset. Both the StrepII tags and the FLAG tag are detectable in western analysis (Figure S3). Identification of NVen210 fusions can be accomplished using the many available commercial YFP/GFP antibodies. Although not illustrated here, our mVenus210 system also should be amenable to multi-colour BiFC, which allows the simultaneous detection of one protein interacting with multiple other proteins, since the mVenus fragment used in CVen210 is 100% identical to the corresponding C-terminal fragment in CFP (e.g. mTurquoise2) as well as GFP. In multi-colour BiFC, the fragments employed as the N-termini determine the emission spectra (Hynes *et al.*, 2011).

Assessment of our pDOE BiFC system using MLO1, CaM1, and CML40

We found that the mVenus210 system significantly outperformed all other systems tested and reduced the background signal to undetectable levels. The GPA1:NmVen210 and MLO1:NmVen210 parent vectors, each expressed without a fused protein in MCS3, showed no fluorescent background signal (Figure 4a,b; see Figure S4 for corresponding brightfield images). Very infrequently, the MLO1:NmVen210 parent vector infiltrations would show some weak background signal in the YFP channel at extended times post-infiltration (3–5 days), but this generally only occurred proximal to the infiltration site, was variable in appearance and subcellular pattern, and occurred in cells that often looked unhealthy. The MLO1-CaM1 positive control interaction was indeed positive, producing distinct BiFC signal at the cell periphery (Figure 4c).

As the next test of this pDOE mVenus210 BiFC system, we focused on the interaction of MLO1 with calmodulin-like proteins. Calmodulin proteins are highly conserved, with most metazoan organisms sharing a single protein isoform with 99–100% identity (Friedberg and Rhoads, 2001). The Arabidopsis proteome contains four typical calmodulin isoforms sharing 96–99% sequence identity to each other and approximately 91% identity to the vertebrate CaM sequence (McCormack and Braam, 2003). Unlike metazoans, plants also have a large family of calmodulin-like sequences (CMLs) with the Arabidopsis family comprising 50 CMLs sharing 16–75% identity with Arabidopsis CaM2 (McCormack and Braam, 2003). The near identity of typical CaMs and the highly conserved nature of the MLO CaMBD (Kim *et al.*, 2002) suggests that uncharacterized MLOs and other proteins containing similar CaM binding domains should interact with typical CaMs. What has not been assessed is the promiscuity of the MLO1 CaMBD; i.e. does MLO1 associate solely with typical CaMs, or can members of the divergent CML family also bind the MLO1 CaMBD? We investigated this question using CML40, which shares only 25% identity and 56% similarity with CaM2, (McCormack *et al.*, 2005), is missing two of the four Ca^{2+} binding EF hands that identify canonical CaMs, and has atypical residues at conserved sites within one EF-hand that suggest weaker overall Ca^{2+} binding coupled with an increased affinity for Mg^{2+} (McCormack and Braam, 2003). We found that CML40 does interact with MLO1 in the same subcellular pattern as the MLO1–CaM interaction, although with a qualitatively weaker BiFC signal (Figure 4d). Independent *in vivo* assays using the yeast-based split-ubiquitin system (Obrdlik *et al.*, 2004) confirmed these interactions (Figure S5). These data suggest that CMLs may fine tune the functions of CaMBD proteins, perhaps in response to cation ratios.

We wondered whether our pDOE base vectors would also show no self-assembly, but like most, if not all BiFC systems, the unfused fragments produced some fluorescence (Figure S6), which simply further emphasizes the utility of our parent vector concept. This self-assembly potential is orientation specific and is significantly less when CVen210 is positioned downstream of the MCS, regardless of the NmVen210 fragment orientation (Figure S6a,b). Finally, we used our pDOE vector to perform a head-to-head comparison of the initial 173/155 fragment pair and our mVen210 system, and confirmed that the pDOE mVen210 system remarkably reduces background non-specific signal (Figure S7).

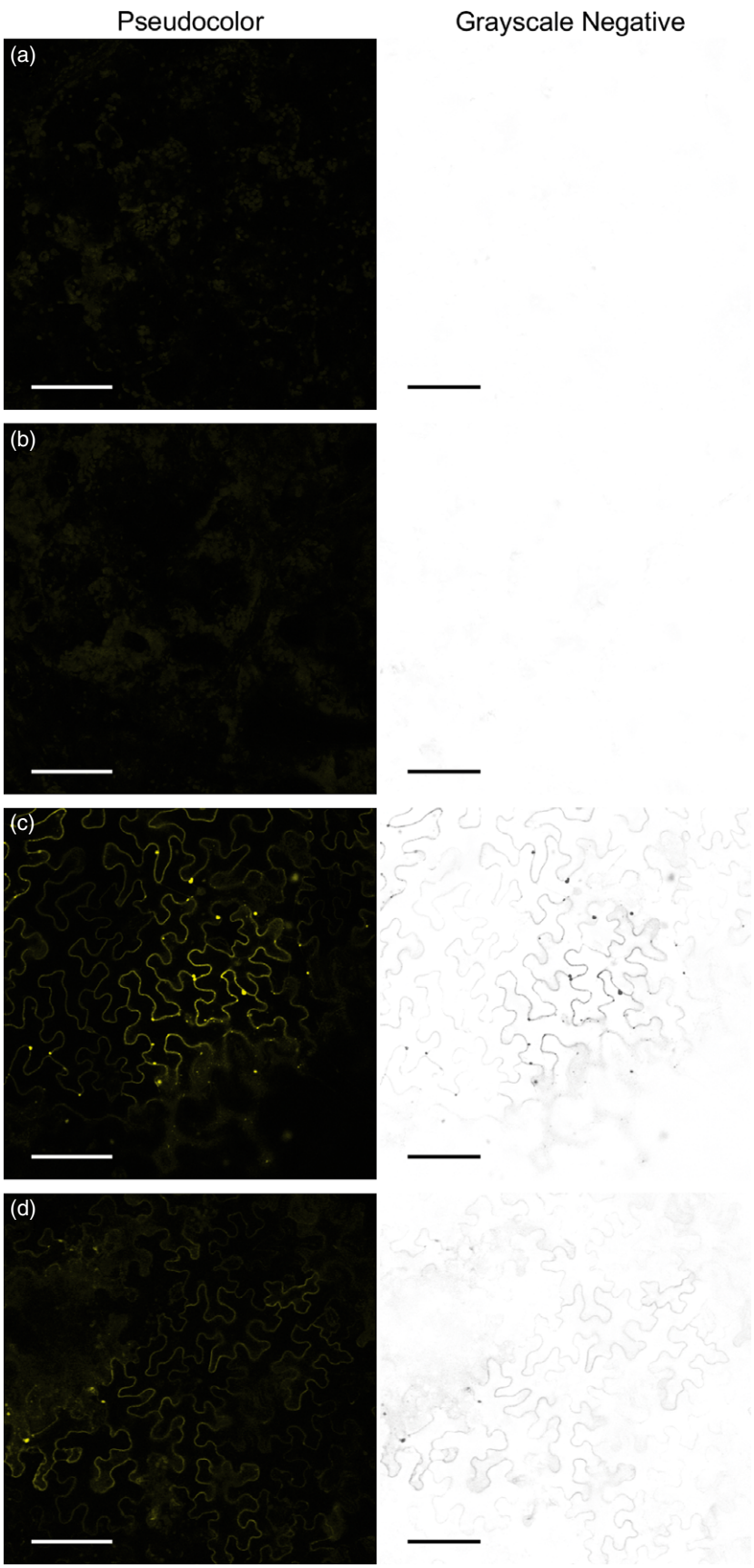

Figure 4. The pDOE–mVenus210 system significantly improves *in planta* BiFC.
(a) GPA1:NmVen210–X:CVen210 parent vector shows zero background signal.
(b) MLO1:NmVen210–X:CVen210 parent vector shows zero background signal.
(c) MLO1:NmVen210 interacts with CaM1:CVen210.
(d) MLO1:NmVen210 interacts with CML40:CVen210.
The MLO1–CML40 interaction is weaker than the MLO1–CaM1 interaction, and could be misconstrued as non-specific signal if observed in the NVen173/155 or NVen155/155 systems. mVenus channel raw data were doubled equally for all images to confirm the lack of signal in (a) and (b). Autofluorescence in the 650–710 nm range was subtracted while processing the grayscale images. Brightfield images are provided in Figure S4. *Nicotiana benthamiana* leaves were agroinfiltrated at an optical density of 0.025 and imaged 45 h later. Scale bars = 100 μm.

Heterotrimeric G-protein subunit assembly in the pDOE BiFC system

As a second, functionally independent, test of our pDOE mVenus210 BiFC system, we applied our system to the well-established eukaryotic heterotrimeric G-protein complex which occupies a central regulatory position in modulating internal and external cellular cues in both metazoan and plant systems (Jones and Assmann, 2004). The complex comprises a cytosolic but lipid-anchored GDP/GTP-binding Gα subunit with intrinsic GTPase activity, and a dimer composed of Gβ, a beta-transducin-type protein with seven WD-40 repeats, and a small lipid-anchored Gγ subunit. The classic paradigm of G-protein signaling entails a signaling cascade wherein the assembled Gαβγ heterotrimer interacts with a plasma membrane-spanning G-protein-coupled receptor which senses and transduces extracellular signals, leading to a dissociation of the G-protein complex into a free Gα subunit and a free Gβγ dimer, which signal to downstream effectors. The complex is returned to its 'resting state' via the intrinsic GTPase activity of Gα and a re-association of the heterotrimer. Other G-protein signaling paradigms are possible in metazoa and plants (Urano *et al.*, 2013; Beninca *et al.*, 2014). In plant systems G-proteins play major roles in morphogenesis, hormone signaling, homeostasis, and pathogenesis (Urano *et al.*, 2013). Although many physiological outputs from G-protein signaling are understood, the exact regulatory mechanisms that affect G-protein complex assembly, disassociation, and downstream signaling are incompletely known, especially in plants.

In contrast with metazoan systems, which contain multiple isoforms of each G-protein subunit [e.g. humans have 16 Gα, 5 Gβ, and 12 Gγ subunits (McCudden *et al.*, 2005)] that can combine into hundreds of distinct signaling complexes, Arabidopsis has only one canonical Gα subunit (GPA1), one Gβ subunit (AGB1) and three Gγ subunits (AGG1, AGG2, and AGG3) which combine to form only three distinct complexes (Thung *et al.*, 2012). The *in planta* interaction of AGB1 and AGG1, and of GPA1 and AGG1 in the presence of AGB1 has been visualized by FRET, but direct interaction between GPA1 and AGB1 could not be shown by FRET even in the presence of a Gγ subunit (Wang *et al.*, 2008), leaving unanswered a fundamental question concerning the nature of the G-protein heterotrimer in plants: do Gα and Gβ physically interact in plants, as they do in mammalian and yeast systems, or not?

As a step toward better understanding the configuration of the G-protein heterotrimer in living plant cells, we first created an AGB1 parent vector in the NmVen210:AGB1 configuration and confirmed dimerization of AGB1 with AGG1, AGG2, and AGG3 in the CVen210:X orientation (Figure S8), where 'X' stands for the translated MCS and linker.

We next sought to evaluate the direct interaction of GPA1 and AGB1, utilizing a test construct of GPA1:NmVen210—AGB1:CVen210, but like the parent construct, the test construct yielded negative results, even when co-infiltrated with pDOE–$G\gamma_1\gamma_2$, a construct expressing untagged AGG1 and AGG2. Since the C-terminal tagging strategy for GPA1 failed, since an αb–αc loop insertion of CFP into GPA1 could not provide FRET with AGB1 N-terminally tagged with YFP in a previous report (Wang *et al.*, 2008), and since the GPA1 and AGB1 N-termini are located on opposite sides of the complex according to the *in vitro* crystallization data of a mammalian heterotrimer (McCudden *et al.*, 2005), we inserted a linker-adapted NmVen210 fragment into the αB–αC loop of GPA1 (GPAL) (Gibson and Gilman, 2006). This created a parent vector consisting of GPAL—CVen210:X. After verifying that the GPAL parent vector showed zero to negligible background fluorescence (Figure 5), we inserted AGB1 into MCS3 and agroinfiltrated the GPAL—CVen210:AGB1 construct with and without pDOE–$G\gamma_1\gamma_2$. Without the $G\gamma_1\gamma_2$ construct, again no fluorescence could be observed (Figure 5c). However, addition of $G\gamma_{1,2}$ enabled visualization of a strong and specific BiFC signal at the plasma membrane (Figure 5d,e). To clarify the roles of the Gγ proteins in heterotrimer assembly, we next tested the ability of singly expressed AGG1, AGG2, and AGG3 to facilitate GPA1–AGB1 interaction and found positive results for all three (Figure 5f–h). These experiments show that our pDOE system is functional even with an internally fused NmVen210, and demonstrate that GPA1 interaction with AGB1 is dependent on sufficient levels of a Gβγ dimer; this dependency may partially explain the congruency of *agb1* and triple Gγ mutant phenotypes (Thung *et al.*, 2012).

GPA1 interacts with PLDα1 but not with PLDα1 substitution mutants

As a third test of our optimized BiFC system, we chose to investigate the published interaction of Arabidopsis GPA1 and the phospholipase PLDα1. Bacterially expressed tobacco Gα and PLDα interact *in vitro* but interaction *in vivo* has not been tested. (Lein and Saalbach, 2001). A PLDα1 'EKF' tripeptide motif, purportedly similar to the DRY motif found in mammalian G protein-coupled receptors (GPCRs), was identified as a critical domain for GPA1–PLDα1 interaction, and residue substitutions decreased GPA1 inhibition of PLDα1 activity *in vitro* (Zhao and Wang, 2004). The putative 'DRY' motif of Arabidopsis PLDα1 was subsequently described as being misannotated (Johnston *et al.*, 2008); therefore a more appropriate name for this site is the PLDα1 EKF tripeptide. Nevertheless, a more recent comparison does show that rice PLDα1 has a similar sequence, ERF, at the same relative position (Zhao and

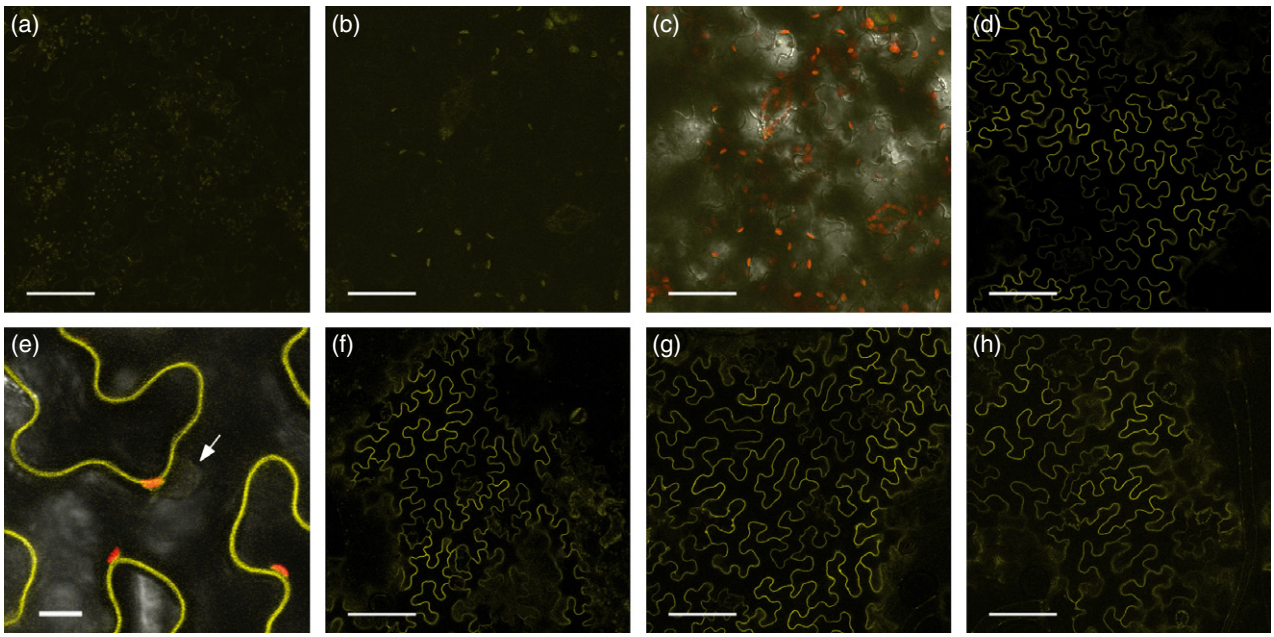

Figure 5. GPA1 with an internal fusion of NmVenus210 (GPAL) specifically interacts with CVen210:AGB1 when co-expressed with untagged AGG1, AGG2, or AGG3.
(a) The GPAL parent vector produces zero to negligible background.
(b) When assayed with only AGB1 the signal is absent; only non-specific autofluorescence can be seen in the mVenus channel.
(c) Signal in the mVenus channel for GPAL with only AGB1 overlaps autofluorescence from chloroplasts.
(d) GPAL–AGB1 co-expression with AGG1 and AGG2 produces strong BiFC signal specifically at the cell periphery.
(e) BiFC signal from GPAL–AGB1 does not accumulate in the nucleus.
(f) Singly co-expressed AGG1 assists GPAL–AGB1 interaction.
(g) Singly co-expressed AGG2 assists GPAL–AGB1 interaction.
(h) Singly co-expressed AGG3 assists GPAL–AGB1 interaction.
Nicotiana benthamiana leaves were agroinfiltrated at a final optical density of 0.02 for GPAL–AGB1 and 0.03 for AGGs, and imaged 42–44 h later. Yellow = mVenus BiFC, red = autofluorescence. White arrow in (e) marks the nucleus. Scale bars: 100 μm except the scale bar in (e) = 10 μm.

Wang, 2013), suggesting physiochemical conservation. Additional biochemical and plant physiological data support the Arabidopsis PLDα1 EKF tripeptide as important for ABA inhibition of stomatal opening (Mishra *et al.*, 2006) but the interaction of GPA1 and PLDα1 in living plant cells has never been evaluated, and the physiological relevance of the GPA1–PLDα1 interaction has been questioned (Urano *et al.*, 2013).

We cloned Arabidopsis wild-type PLDα1 into MCS3 of our GPA1 parent vector to produce a BiFC construct in the GPA1:NmVen210—PLDα1:CVen210 configuration. Using site-directed mutagenesis, we also created PLDα1 mutant versions containing an EKF→GAA substitution (PLDm1) and a longer EKFRVY→GAASGS substitution (PLDm2) which also destroys part of an adjacent highly conserved hydrophobic patch. Importantly, these single vector constructs all contain an integrated Golgi-localized mTurquoise2 marker (XT-Golgi-mTq2) to specifically identify transformed cells. Agroinfiltration into *N. benthamiana* leaves showed that GPA1 can interact with wild-type PLDα1 in living plant cells and that the resultant BiFC signal localizes to the cell periphery. Figure 6 shows an image that is representative of six independent experiments. Interaction assays of GPA1 with the PLDm1 residue substitution mutant in the same six experiments were devoid of BiFC signal, confirming the importance of the PLDα1 EKF/DRY motif in G-protein interaction (Figure 6c, d). We present the GPA1–PLDα1 interaction as a maximum projection of Z-stack images through an isolated cell to show the subcellular localization of the interaction (Figure 6b). Population-level images are presented in Figure S9 which shows low-magnification overviews of an additional four experiments in which GPA1–PLDα1 interaction produced extensive BiFC signal. Parallel tests of GPA1–PLDm1 interaction did not show any BiFC signal (Figure S9), and the Golgi marker confirmed successful transformation in every case (Figure S10). In total, GPA1 interacted with PLDα1 in 100% of experiments (10/10) but did not interact with PLDm1 in any experiments (0/10). PLDα1 and PLDm1 protein abundance was comparable by western analysis (Figure S3a). Notably, careful adherence to low agroinfiltration optical densities (0.005–0.02) was key for PLDα1 and PLDm1 assay optimization, presumably due to the negative consequences of sustained lipase activity; difficulty in working with PLDα1 *in vivo* has been reported previously (Zhao and Wang, 2013).

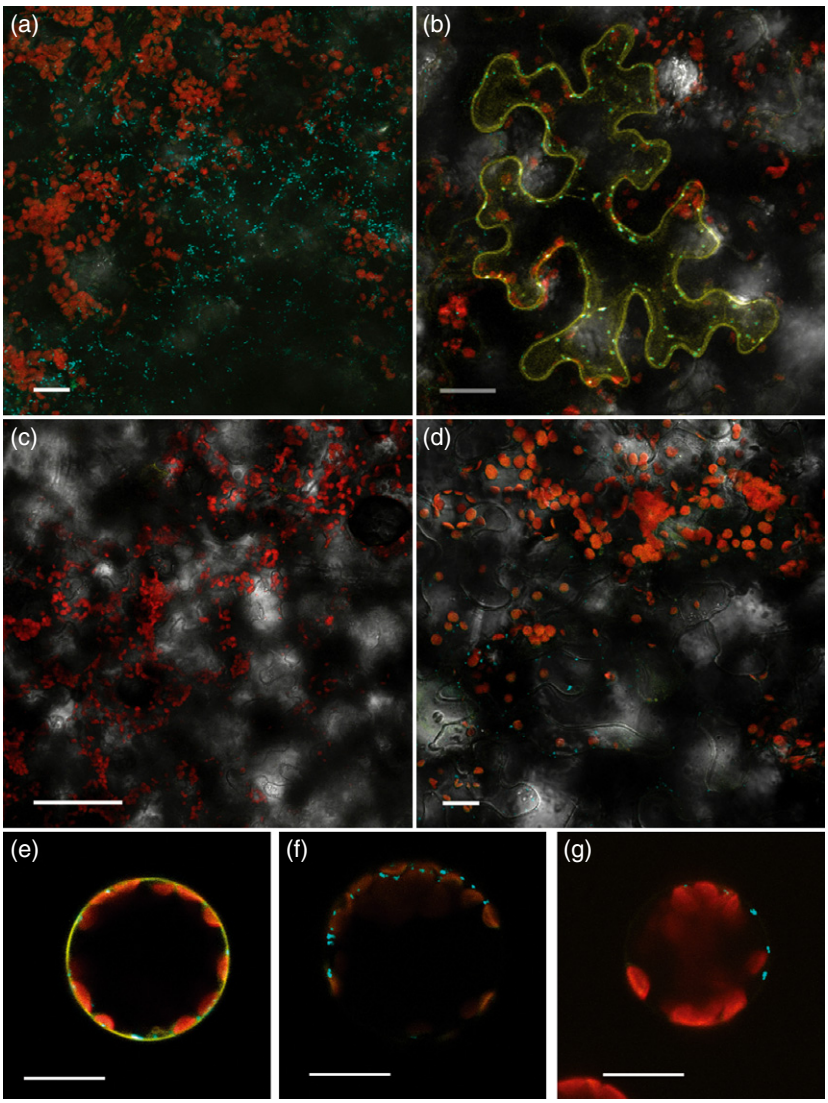

Figure 6. GPA1 interacts with PLDα1, but not with the PLDm1 (EKF→GAA) residue substitution mutant.
(a) The GPA1:NmVen210—X:CVen210 parent vector shows no background BiFC signal even when agroinfiltrated into *Nicotiana benthamiana* leaves at an optical density of 0.2 and imaged 66 h post-infiltration; maximum projection shows blue XT–Golgi–mTq2 signal marking transformed cells.
(b) GPA1:NmVen210 interacts with PLDα1:CVen210; maximum projection shows the signal is only at the cell periphery.
(c) GPA1:NmVen210 appears not to interact with PLDm1:CVen210, but the presence of transformed cells cannot be confirmed when p19 is in MCS2.
(d) GPA1:NmVen210 does not interact with PLDm1:CVen210; the mTq2 Golgi marker clearly identifies transformed cells, confirming a true negative event even when few cells are transformed.
(e) GPA1:NmVen210 interaction with PLDa1::CVen210 occurs in Arabidopsis *gpa1-3* mesophyll protoplasts.
(f) GPA1:NmVen210 does not interact with PLDm1:CVen210 in Arabidopsis *gpa1-3* mesophyll protoplasts.
(g) GPA1:NmVen210 also does not interact with PLDm2 in Arabidopsis *gpa1-3* mesophyll protoplasts. Agroinfiltration of *N. benthamiana* at very low optical densities (0.005–0.01) allows interaction assays (b, d) in well-isolated cells 44 h post-infiltration. Arabidopsis protoplasts were imaged 12 h post-transformation. Maximum projections (a) ×20 and (b) ×40 magnifications with digital zoom. Single focal plane images at (c, d) ×40 and (e–g) at ×63 magnifications. Identical mVenus channel parameters for (e–g) allow direct comparison. All scale bars = 20 μm except (c) = 50 μm. Yellow = mVenus BiFC, blue = mTq2 Golgi marker, red = autofluorescence.

We next performed these interaction assays using an alternative system, transient transformation of Arabidopsis mesophyll protoplasts. Protoplasts were derived from *gpa1-3*, a GPA1 knockout line. These experiments confirmed that GPA1 interacts with PLDα1, but not with the PLDm1 or PLDm2 mutant proteins (Figure 6e–g). Successful transformation was confirmed via visualization of the XT–Golgi–mTq2 marker (e.g. Figure 6a,d,f,g), illustrating the usefulness of the pDOE system in distinguishing false-negative results (e.g. arising from lack of transformation) from true negative results. Moreover, we also demonstrated interaction of PLDα1 and GPA1 via biolistic transformation of Arabidopsis *gpa1-3* leaves (Figure S11).These experiments illustrate that our pDOE system is not restricted to use in *N. benthamiana*. The applicability of the pDOE system to protoplast and biolistic transformation is particularly valuable given that transient transformation of Arabidopsis offers the possibility to assess protein–protein interactions in different genetic backgrounds.

AGB1–AGG dimers interact with PLDα1

Although a direct interaction between metazoan PLD and Gα has, to our knowledge, not been described, metazoan PLD activity has been shown to be negatively regulated by $G\beta_1\gamma_1$ and $G\beta_1\gamma_2$ *in vitro* and by $G\beta_1\gamma_1$ *in vivo* (Preininger *et al.*, 2006). This suggests that a signaling mechanism common to eukaryotes might exist wherein PLDs are regulated by direct interaction with both Gα and Gβγ. With evidence that Arabidopsis PLDα1 can interact with GPA1 *in planta*, we sought to determine if PLDα1 could also interact with plant Gβγ dimers. We created four parent vectors containing AGB1 in MCS1 to allow evaluation of all N- and C-terminal tag combinations, and then created a test set by inserting PLDα1 into MCS3. Since the XT–Golgi–mTq2

transformation control is a critical component for assessing negative results, we supplied XT–Golgi–mTq2 in MCS2 and exogenous untagged gamma subunits via the same pDOE–G$\gamma_1\gamma_2$ vector that successfully facilitated GPA1–AGB1 interaction. We found that AGB1 can interact with PLDα1, but strongly only when NmVen210 is fused to the N-terminus of AGB1 (Figure 7). Initial end-point assays showed that CVen210 fusions to both termini of PLDα1 each interacted with NmVen210:AGB1 with similar strength, but time series experiments identified NmVen210:AGB1—CVen210:PLDα1 to be the qualitatively more robust interaction. Interestingly, this configuration is opposite of the GPA1–PLDα1 interaction configuration, which showed strong interaction when both proteins were C-terminally tagged. Identifying the most robust configuration for AGB1–PLDα1 BiFC signal allowed us to then ask whether the EKF→GAA mutation would interfere with the interaction. We created the NmVen210:AGB1—CVen210:PLDm1 test construct and found that mutation of the EKF residues clearly prevented the accumulation of BiFC signal at optimum time points (Figure 8b), and produced at most extremely weak signal even at extended time points (Figure 8d). The possible regulation of PLDα1 activity by AGB1 is a topic for future research; it is interesting to speculate that either AGB1 or GPA1 might have the dominant regulatory role when complexed in the heterotrimer, but that each may differentially regulate PLDα1 when dissociated into the free Gα subunit and G$\beta\gamma$ dimer.

CONCLUSIONS

Our experimentation using the currently available BiFC systems and fragment pairs in binary vectors demonstrated a need to reduce background signal from non-specific reassembly in order to increase confidence in both true positives and true negatives. Our extensive *in planta* analysis of BiFC fragments and our identification that the mVenus fluoroprotein split at residue 210 performs efficiently and with remarkably reduced background signal significantly advance BiFC analysis in plants. Using our pDOE BiFC system we were able to show that a divergent CML can interact with MLO1, and that the direct interaction of GPA1 with AGB1 is highly dependent on the presence of a stoichiometrically balanced Gγ subunit. We also demonstrate that GPA1 and AGB1 each interact with PLDα1, but not with PLDα1 'DRY' motif mutants. Importantly, our XT–Golgi–mTq2 transformation control unobtrusively labels transformed cells, and provides a landmark to identify these cells when BiFC signal is absent.

The utility of our single vector system lies in the streamlined integration of candidate interacting partners and the capability to express two test proteins in each and every cell that is transformed; a key asset for scoring large screens. As in any genetically encoded interaction system, auto-activation by the gene of interest is possible, and the relative 'stickiness' of new parent vectors always should be assessed. When combined with protoplast or biolistic transformation, our pDOE BiFC system allows interaction assays to be performed in Arabidopsis or other plant species not amenable to agroinfiltration. Further, these protein–protein interactions can be assessed in natural genetic variants or mutant backgrounds, allowing the possibility to identify unique requirements or regulatory modes necessary for interaction.

EXPERIMENTAL PROCEDURES

Vector set creation

We chose to initially create and optimize vectors in which both proteins are tagged on the C-terminus. Vectors with other orientations and combinations were created using the finalized initial set (Figure 2 and Methods S2). A list and full details of vector set creation and utilization are presented in supporting information (Methods S1) and a summary is presented here. Primers for colony polymerase chain reaction (PCR), sequencing, and discriminating between mTurquoise2 and mVenus are presented in Table S1.

In brief, we utilized the vector backbone of pFGC5941 as a scaffold to hold two expression cassettes, each comprising an identical promoter (*Cauliflower Mosaic Virus* 35S or *Ubiquitin 10*) fused to an Omega viral translation enhancer, followed by a segment of unique MCS and fusion protein fragments. All expression cassettes for MCS1 are terminated by the OCS 3′ terminator and all expression cassettes for MCS3 are terminated by the NOS terminator. The original 2′ MAS promoter-driven BASTA resistance cassette was annotated as MCS2, and was replaced with the p19 silencing suppressor or the XT–Golgi–mTq2 transformation control, which was constructed by fusing the N-terminal transmembrane domain containing 36 amino acids of AtXylT (Pagny *et al.*, 2003; Saint-Jore-Dupas *et al.*, 2006) to the N-terminus of mTq2. Our choice of transformation control was based on its unobtrusive signal, but it easily can be replaced by alternative markers or ORFs. All pDOE BiFC vectors contain N-Venus fragments in MCS1 and C-Venus fragments in MCS3. Subcellular localization vectors have mTq2 in MCS1 and mVenus in MCS3. Vectors were completely sequenced: GenBank accession #KM507041 to KM507060 (www.ncbi.nlm.nih.gov/genbank). Plasmids will be distributed through TAIR (www.arabidopsis.org).

Vector utilization

Genes of interest are optimally cloned into MCS1 to create a 'parent vector' and target genes are cloned into MCS3; the reverse is an option but is not optimal for large-scale one-to-many screens and therefore not addressed here. Target ORF cloning into MCS3 is optimally performed using our rare-cutting *San*DI site, which is compatible with inserts cut with *Rsr*II, *Ava*II, and *Ppu*MI, and allows cloning of ORFs for approximately all 30 000 non-redundant Arabidopsis proteins into a single open vector purification. A detailed description of construction strategies is provided in supplemental methods (Methods S1 and S2). MCS2 is reserved for lower level expression, via the MAS promoter, of regulatory proteins (e.g. p19), of transformation controls (e.g. XT–Golgi–mTq2), or of accessory proteins as desired. After creating the parent vector, the process is streamlined, with the time from candidate insertion to BiFC data collection as short as 8–10 days.

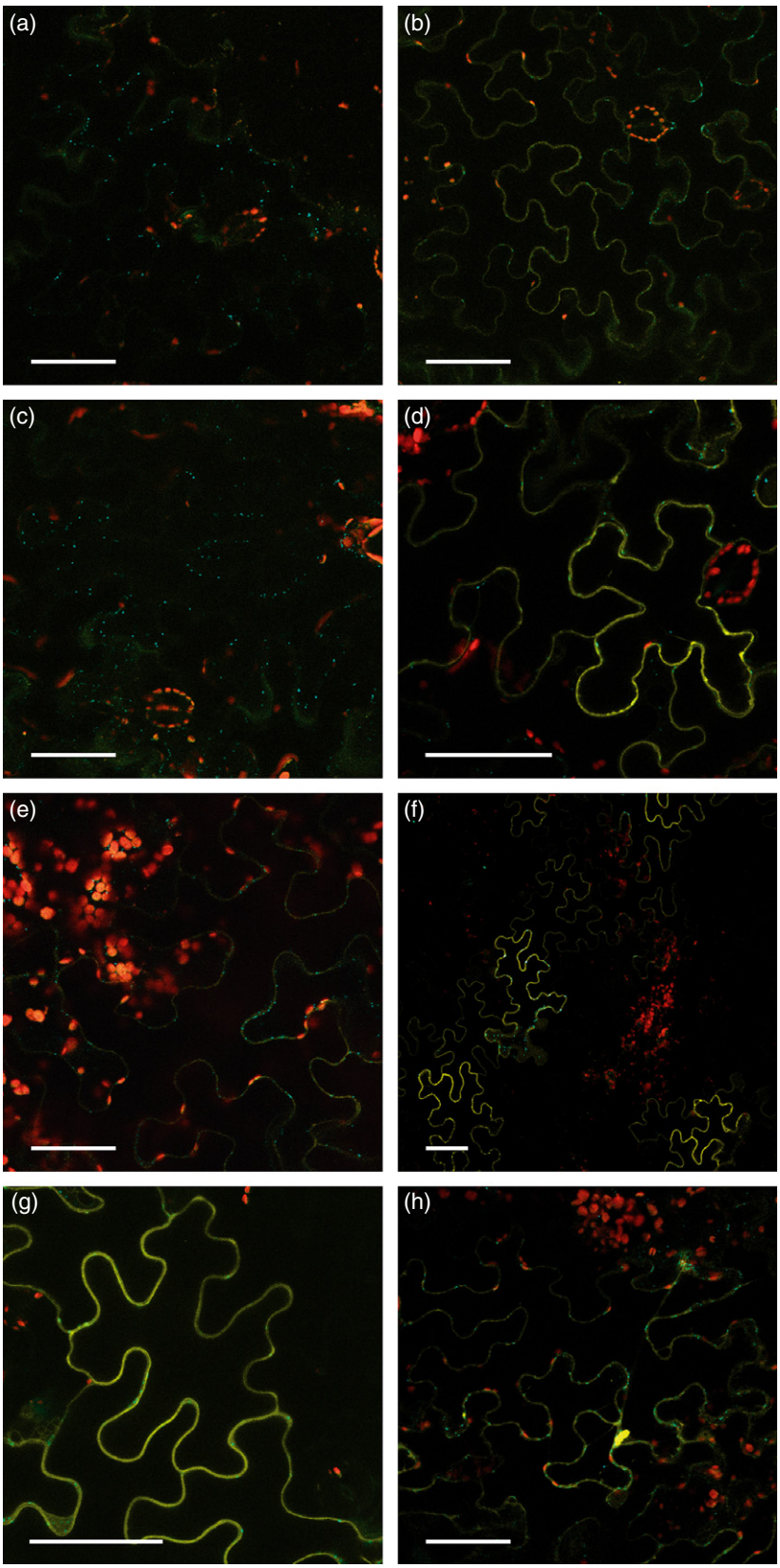

Figure 7. AGB1 interacts with PLDα1 and the interaction shows orientation specificity in the mVen210 BiFC system.
All assays except (h) were performed with co-infiltration of pDOE Gγ1γ2. In (a), (c), and (e), successful transformation is evident from the blue mTq2 Golgi signal.
(a) AGB1:NmVen210 fusion shows no background signal with X:CVen210.
(b) AGB1:NmVen210 interacts with PLDα1:CVen210.
(c) NmVen210:AGB1 shows no background signal with X:CVen210.
(d) NmVen210AGB1 interacts with PLDα1:CVen210.
(e) NmVen210:AGB1 shows zero to very little background signal with CVen210:X.
(f) NmVen210:AGB1 interacts with CVen210:PLDα1.
(g) The NmVen210:AGB1 interaction with CVen210:PLDα1 does not localize to the nucleus with co-expression of untagged AGG1 and AGG2.
(h) Without co-expressed Gγ subunits, signal from the NmVen210:AGB1 interaction with CVen210:PLDα1 appears in the nucleus. *Nicotiana benthamiana* leaves were agroinfiltrated at an optical density of 0.04, BiFC signal development was evaluated every 4 h from 36 to 68 h, and images were taken 68–70 h post-infiltration to determine the optimum fusion protein orientation for interaction. All scale bars = 50 μm. Yellow = mVenus BiFC, blue = mTq2 Golgi marker, red = autofluorescence.

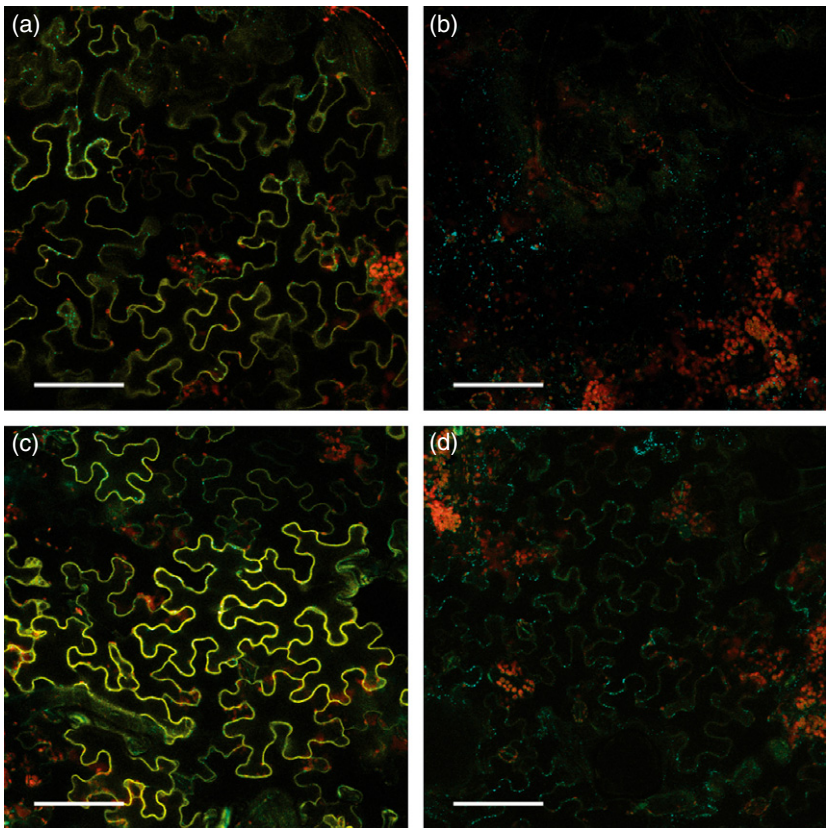

Figure 8. AGB1 does not interact, or interacts extremely weakly, with the PLDα1 m1 (EKF→GAA) residue substitution mutant.
In (b) and (d), successful transformation is evident from the blue mTq2 Golgi signal.
(a) NmVen210:AGB1 interacts strongly with CVen210::PLDα1 at 48 h.
(b) NmVen210:AGB1 and CVen210:PLDm1 do not produce any BiFC signal at 48 h.
(c) NmVen210:AGB1—CVen210:PLDα1 BiFC signal is very high at the post-optimal timepoint of 65 h.
(d) NmVen210:AGB1 and CVen210:PLDm1 produce zero to extremely weak BiFC signal at the late timepoint of 66 h. *Nicotiana benthamiana* leaves were agroinfiltrated at a final optical density of 0.02. Scale bars = 100 μm. Yellow = mVenus BiFC, blue = mTq2 Golgi marker, red = autofluorescence.

Agroinfiltration, protoplast, and biolistic transformation

Vectors were electroporated into *Agrobacterium* strain GV3101 pMP90 and selected on LB agar supplemented with 50 μg ml^{-1} kanamycin and 15 μg ml^{-1} gentamicin. After 2–3 days' growth, several colonies (equivalent to a small *E. coli* plasmid mini-prep cell pellet) were carefully harvested from the plate, suspended in LB agar and incubated at 29°C for 1–2 h with 100 μM acetosyringone (Sigma-Aldrich, www.sigmaaldrich.com). The cells were pelleted, washed with, and resuspended in, infiltration buffer (10 mM MES, 10 mM $MgCl_2$, pH 5.6 with KOH, 100 μM acetosyringone). Infiltrations were performed using exactly equal OD_{600} values for all comparative assays. OD values for pDOE test vectors were generally ≤ OD_{600} = 0.03 except for negative controls which were occasionally tested up to OD_{600} = 0.40. The pDOE system allowed visualization of positive interactions using OD_{600} values as low as 0.001; low infiltration densities facilitate fine detail analyses (Tilsner *et al.*, 2013). Agroinfiltration based BiFC assays were assessed with and without co-infiltration of 35S:p19 with no changes in results. Protoplast transformation was performed using 5 and 10 μg plasmid DNA essentially as described by Yoo *et al.* (2007). Biolistic transformation was performed as previously described (Li *et al.*, 2000).

Nicotiana benthamiana and *Arabidopsis thaliana* plants were grown in Metro-Mix 360 (Sun-Gro Horticulture, www.sungro.com) in growth chambers with 10-h light/14-h dark cycles, 140 μmol photons m^{-2} sec^{-1}, 20°C. BiFC control and test infiltrations were performed on the same leaf, and duplicate infiltrations were performed on at least three plants within a single experimental assay. Typically, new construct sets were screened once or twice to identify their general characteristics (e.g. signal appearance and strength) before performing at least three to six independently replicated assays, i.e. on separate days. BiFC assays were performed as time-courses with observations from 26 to 72 h, and all comparative timepoint samplings were performed together. 35S-driven expression occurred earlier than UBQ10 promoter-driven expression (e.g. Figure S8). We note that plant health and physiological status greatly affect the kinetics of protein expression and signal appearance (e.g. Figure S5). Importantly we note that acquisition times are relevant for direct comparison only when plant materials are equivalent; plants of different ages or physiological status can express proteins at different rates, and protein stability may vary in differing *in vivo* environments.

Confocal microscopy and immunoblot analysis

Confocal microscopy was performed using a Zeiss LSM 510 META laser scanning microscope (Carl Zeiss, Thornwood, NY, USA). Argon laser line excitation wavelength and emission bandpass filter wavelengths for mTq2 and mVenus were 458 nm and 480–520 nm, and 488 nm and 500–550 nm, respectively. Chlorophyll autofluorescence was detected, in parallel with mTq2 acquisition, using a 650–710 nm bandpass filter. Image acquisition parameters (e.g. laser power, pinhole, detector gain, etc.) and sampling time post-infiltration were held constant within an experiment (i.e. within each figure). Raw BiFC data for the mVenus channel were not altered beyond equal signal increases (by equally decreasing the lower dynamic range value) in the ZEISS ZEN 2010 software (www.zeiss.com) within an experiment, and subtraction of autofluorescence where noted.

Immunoblots were performed using a ThermoFisher FLAG–HRP antibody (FG4R, MA1–91878, www.thermoscientific.com) and IBA StrepTactin–HRP (2-1502-001, www.iba-lifesciences.com) and

the manufacturer's Strep-tag detection protocol. Split-ubiquitin assays were performed as previously detailed (Gookin and Bendtsen, 2013).

ACKNOWLEDGEMENTS

This research was supported by NSF grant NSF-MCB 1121612 to S.M. Assmann and R. Albert. We thank Ms. Yunqing Yu, Dr. Matthew Milner, and Dr. Daisuke Tsugama for beta testing our BiFC system in their research.

SUPPORTING INFORMATION

Additional Supporting Information may be found in the online version of this article.

Figure S1. Unfused C-terminal NVen173/155 fragments produce strong signal.

Figure S2. NVen155 point mutations variably reduce but do not eliminate mVenus self-assembly even at an early sampling time (40 h post-infiltration).

Figure S3. The PLDα1 and PLDm1 proteins are detectable at similar levels in BiFC assays, and both epitope tags are functional.

Figure S4. Bright field images for main text Figure 4.

Figure S5. *In vivo* confirmation of MLO1 interaction with a typical calmodulin (CaM3) and with a calmodulin-like protein (CML40) in the membrane based split-ubiquitin yeast two-hybrid system.

Figure S6. pDOE BiFC base vectors with two empty cloning cassettes show weaker self-assembly in the X:CVen orientation than in the CVen:X orientation.

Figure S7. Direct comparison in the pDOE vector shows the NmVen210 system remarkably reduces background signal compared to the 173/155 pair.

Figure S8. AGB1 interacts with all three *Arabidopsis* Gγ subunits in plant cells.

Figure S9. Population level confirmation that GPA1 interacts with PLDα1, but not with the PLDm1 (EKF→GAA) residue substitution mutant, in the pDOE mVenus210 BiFC system.

Figure S10. The XT-mTq2-Golgi marker confirms transformation of the GPA1:NVen210—PLDm1:CVen210 vector and demonstrates that the plants are capable of expressing exogenous protein.

Figure S11. Confirmation of the GPA1-PLDα1 interaction in *Arabidopsis gpa1-3* mutants using biolistic transformation.

Table S1. Primers for colony PCR, sequencing, and discriminating between mTurquoise2 and mVenus.

Method S1. Supporting experimental details and pDOE system description.

Method S2. Detailed pDOE vector schematics and cloning strategies.

REFERENCES

Beninca, C., Planaguma, J., de Freitas Shuck, A. *et al.* (2014) A new non-canonical pathway of Gαq protein regulating mitochondrial dynamics and bioenergetics. *Cell. Signal.* **26**, 1135–1146.

Berendzen, K.W., Bohmer, M., Wallmeroth, N., Peter, S., Vesic, M., Zhou, Y., Tiesler, F.K., Schleifenbaum, F. and Harter, K. (2012) Screening for *in planta* protein-protein interactions combining bimolecular fluorescence complementation with flow cytometry. *Plant Methods*, **8**, 25.

Devoto, A., Piffanelli, P., Nilsson, I., Wallin, E., Panstruga, R., von Heijne, G. and Schulze-Lefert, P. (1999) Topology, subcellular localization, and sequence diversity of the Mlo family in plants. *J. Biol. Chem.* **274**, 34993–35004.

Evers, T.H., van Dongen, E.M., Faesen, A.C., Meijer, E.W. and Merkx, M. (2006) Quantitative understanding of the energy transfer between fluorescent proteins connected via flexible peptide linkers. *Biochemistry*, **45**, 13183–13192.

Friedberg, F. and Rhoads, A.R. (2001) Evolutionary aspects of calmodulin. *IUBMB Life*, **51**, 215–221.

Gehl, C., Waadt, R., Kudla, J., Mendel, R.-R. and Hänsch, R. (2009) New GATEWAY vectors for high throughput analyses of protein-protein interactions by bimolecular fluorescence complementation. *Mol. Plant*, **2**, 1051–1058.

Gibson, S.K. and Gilman, A.G. (2006) Giα and Gβ subunits both define selectivity of G protein activation by α2-adrenergic receptors. *Proc. Natl Acad. Sci. USA*, **103**, 212–217.

Goedhart, J., van Weeren, L., Hink, M.A., Vischer, N.O., Jalink, K. and Gadella, T.W. Jr (2010) Bright cyan fluorescent protein variants identified by fluorescence lifetime screening. *Nat. Methods*, **7**, 137–139.

Gookin, T.E. and Bendtsen, J.D. (2013) Topology assessment, G protein-coupled receptor (GPCR) prediction, and *in vivo* interaction assays to identify plant candidate GPCRs. *Methods Mol. Biol.* **1043**, 1–12.

Grefen, C., Donald, N., Hashimoto, K., Kudla, J., Schumacher, K. and Blatt, M.R. (2010) A ubiquitin-10 promoter-based vector set for fluorescent protein tagging facilitates temporal stability and native protein distribution in transient and stable expression studies. *Plant J.* **64**, 355–365.

Groth, A., Corpet, A., Cook, A.J., Roche, D., Bartek, J., Lukas, J. and Almouzni, G. (2007) Regulation of replication fork progression through histone supply and demand. *Science*, **318**, 1928–1931.

Hynes, T.R., Yost, E.A., Yost, S.M. and Berlot, C.H. (2011) Multicolor BiFC analysis of G protein βγ complex formation and localization. *Methods Mol. Biol.* **756**, 229–243.

Isogai, M., Kawamoto, Y., Inahata, K., Fukada, H., Sugimoto, K. and Tada, T. (2011) Structure and characteristics of reassembled fluorescent protein, a new insight into the reassembly mechanisms. *Bioorg. Med. Chem. Lett.* **21**, 3021–3024.

Johnston, C.A., Willard, M.D., Kimple, A.J., Siderovski, D.P. and Willard, F.S. (2008) A sweet cycle for Arabidopsis G-proteins: recent discoveries and controversies in plant G-protein signal transduction. *Plant Signal. Behav.* **3**, 1067–1076.

Jones, A.M. and Assmann, S.M. (2004) Plants: the latest model system for G-protein research. *EMBO Rep.* **5**, 572–578.

Kerppola, T.K. (2006) Design and implementation of bimolecular fluorescence complementation (BiFC) assays for the visualization of protein interactions in living cells. *Nat. Protoc.* **1**, 1278–1286.

Kim, M.C., Panstruga, R., Elliott, C., Muller, J., Devoto, A., Yoon, H.W., Park, H.C., Cho, M.J. and Schulze-Lefert, P. (2002) Calmodulin interacts with MLO protein to regulate defence against mildew in barley. *Nature*, **416**, 447–451.

Kodama, Y. and Hu, C.D. (2010) An improved bimolecular fluorescence complementation assay with a high signal-to-noise ratio. *Biotechniques*, **49**, 793–805.

Kodama, Y. and Hu, C.D. (2012) Bimolecular fluorescence complementation (BiFC): a 5-year update and future perspectives. *Biotechniques*, **53**, 285–298.

Lalonde, S., Ehrhardt, D.W., Loque, D., Chen, J., Rhee, S.Y. and Frommer, W.B. (2008) Molecular and cellular approaches for the detection of protein-protein interactions: latest techniques and current limitations. *Plant J.* **53**, 610–635.

Lee, L.Y., Fang, M.J., Kuang, L.Y. and Gelvin, S.B. (2008) Vectors for multi-color bimolecular fluorescence complementation to investigate protein-protein interactions in living plant cells. *Plant Methods*, **4**, 24.

Lein, W. and Saalbach, G. (2001) Cloning and direct G-protein regulation of phospholipase D from tobacco. *Biochim. Biophys. Acta*, **1530**, 172–183.

Li, J., Wang, X.Q., Watson, M.B. and Assmann, S.M. (2000) Regulation of abscisic acid-induced stomatal closure and anion channels by guard cell AAPK kinase. *Science*, **287**, 300–303.

Li, M., Doll, J., Weckermann, K., Oecking, C., Berendzen, K.W. and Schoffl, F. (2010) Detection of *in vivo* interactions between Arabidopsis class A-HSFs, using a novel BiFC fragment, and identification of novel class B-HSF interacting proteins. *Eur. J. Cell Biol.* **89**, 126–132.

Lin, J., Wang, N., Li, Y. *et al.* (2010) LEC-BiFC: a new method for rapid assay of protein interaction. *Biotech. Histochem.* **86**, 272–279.

Mal, T.K., Takahata, S., Ki, S., Zheng, L., Kokubo, T. and Ikura, M. (2007) Functional silencing of TATA-binding protein (TBP) by a covalent linkage

of the N-terminal domain of TBP-associated factor 1. *J. Biol. Chem.* **282**, 22228–22238.

McCormack, E. and Braam, J. (2003) Calmodulins and related potential calcium sensors of Arabidopsis. *New Phytol.* **159**, 585–598.

McCormack, E., Tsai, Y.C. and Braam, J. (2005) Handling calcium signaling: Arabidopsis CaMs and CMLs. *Trends Plant Sci.* **10**, 383–389.

McCudden, C.R., Hains, M.D., Kimple, R.J., Siderovski, D.P. and Willard, F.S. (2005) G-protein signaling: back to the future. *Cell. Mol. Life Sci.* **62**, 551–577.

Mishra, G., Zhang, W., Deng, F., Zhao, J. and Wang, X. (2006) A bifurcating pathway directs abscisic acid effects on stomatal closure and opening in Arabidopsis. *Science*, **312**, 264–266.

Nakagawa, C., Inahata, K., Nishimura, S. and Sugimoto, K. (2011) Improvement of a Venus-based bimolecular fluorescence complementation assay to visualize bFos-bJun interaction in living cells. *Biosci. Biotechnol. Biochem.* **75**, 1399–1401.

Obrdlik, P., El-Bakkoury, M., Hamacher, T. *et al.* (2004) K^+ channel interactions detected by a genetic system optimized for systematic studies of membrane protein interactions. *Proc. Natl Acad. Sci. USA*, **101**, 12242–12247.

Ohashi, K., Kiuchi, T., Shoji, K., Sampei, K. and Mizuno, K. (2012) Visualization of cofilin-actin and Ras–Raf interactions by bimolecular fluorescence complementation assays using a new pair of split Venus fragments. *Biotechniques*, **52**, 45–50.

Olinares, P.D., Kim, J., Davis, J.I. and van Wijk, K.J. (2011) Subunit stoichiometry, evolution, and functional implications of an asymmetric plant plastid ClpP/R protease complex in Arabidopsis. *Plant Cell*, **23**, 2348–2361.

Pagny, S., Bouissonnie, F., Sarkar, M., Follet-Gueye, M.L., Driouich, A., Schachter, H., Faye, L. and Gomord, V. (2003) Structural requirements for Arabidopsis β1,2-xylosyltransferase activity and targeting to the Golgi. *Plant J.* **33**, 189–203.

Preininger, A.M., Henage, L.G., Oldham, W.M., Yoon, E.J., Hamm, H.E. and Brown, H.A. (2006) Direct modulation of phospholipase D activity by Gβγ. *Mol. Pharmacol.* **70**, 311–318.

Saint-Jore-Dupas, C., Nebenfuhr, A., Boulaflous, A., Follet-Gueye, M.L., Plasson, C., Hawes, C., Driouich, A., Faye, L. and Gomord, V. (2006) Plant N-glycan processing enzymes employ different targeting mechanisms for their spatial arrangement along the secretory pathway. *Plant Cell*, **18**, 3182–3200.

Saka, Y., Hagemann, A.I., Piepenburg, O. and Smith, J.C. (2007) Nuclear accumulation of Smad complexes occurs only after the midblastula transition in *Xenopus*. *Development*, **134**, 4209–4218.

Thung, L., Trusov, Y., Chakravorty, D. and Botella, J.R. (2012) Ggamma1 + Ggamma2 + Ggamma3 = Gbeta: the search for heterotrimeric G-protein gamma subunits in Arabidopsis is over. *J. Plant Physiol.* **169**, 542–545.

Tilsner, J., Linnik, O., Louveaux, M., Roberts, I.M., Chapman, S.N. and Oparka, K.J. (2013) Replication and trafficking of a plant virus are coupled at the entrances of plasmodesmata. *J. Cell Biol.* **201**, 981–995.

Urano, D., Chen, J.G., Botella, J.R. and Jones, A.M. (2013) Heterotrimeric G protein signalling in the plant kingdom. *Open Biol.* **3**, 120186.

Vahisalu, T., Puzorjova, I., Brosche, M. *et al.* (2010) Ozone-triggered rapid stomatal response involves the production of reactive oxygen species, and is controlled by SLAC1 and OST1. *Plant J.* **62**, 442–453.

von Stetten, D., Noirclerc-Savoye, M., Goedhart, J., Gadella, T.W. Jr and Royant, A. (2012) Structure of a fluorescent protein from *Aequorea victoria* bearing the obligate-monomer mutation A206K. *Acta Crystallogr. Sect. F Struct. Biol. Cryst. Commun.* **68**, 878–882.

Waadt, R., Schmidt, L.K., Lohse, M., Hashimoto, K., Bock, R. and Kudla, J. (2008) Multicolor bimolecular fluorescence complementation reveals simultaneous formation of alternative CBL/CIPK complexes *in planta*. *Plant J.* **56**, 505–516.

Wang, S., Assmann, S.M. and Fedoroff, N.V. (2008) Characterization of the Arabidopsis heterotrimeric G protein. *J. Biol. Chem.* **283**, 13913–13922.

Witte, C.P., Noel, L.D., Gielbert, J., Parker, J.E. and Romeis, T. (2004) Rapid one-step protein purification from plant material using the eight-amino acid StrepII epitope. *Plant Mol. Biol.* **55**, 135–147.

Yoo, S.D., Cho, Y.H. and Sheen, J. (2007) Arabidopsis mesophyll protoplasts: a versatile cell system for transient gene expression analysis. *Nat. Protoc.* **2**, 1565–1572.

Zacharias, D.A., Violin, J.D., Newton, A.C. and Tsien, R.Y. (2002) Partitioning of lipid-modified monomeric GFPs into membrane microdomains of live cells. *Science*, **296**, 913–916.

Zhao, J. and Wang, X. (2004) Arabidopsis phospholipase Dα1 interacts with the heterotrimeric G-protein α-subunit through a motif analogous to the DRY motif in G-protein-coupled receptors. *J. Biol. Chem.* **279**, 1794–1800.

Zhao, J. and Wang, X. (2013) Biochemical analysis of the interaction between phospholipase Dα1 and GTP-binding protein α-subunit from *Arabidopsis thaliana*. *Methods Mol. Biol.* **1043**, 21–35.

Zhong, S., Lin, Z. and Grierson, D. (2008) Tomato ethylene receptor-CTR interactions: visualization of NEVER-RIPE interactions with multiple CTRs at the endoplasmic reticulum. *J. Exp. Bot.* **59**, 965–972.

Zhou, J., Lin, J., Zhou, C., Deng, X. and Xia, B. (2011) An improved bimolecular fluorescence complementation tool based on superfolder green fluorescent protein. *Acta Biochim. Biophys. Sin. (Shanghai)*, **43**, 239–244.